



Los Alamos

NATIONAL LABORATORY

memorandum

LANSCCE Division

To/MS: Distribution

From/MS: James H. Billen/H817

Phone/FAX: 7-6627/5-2904

Email: JBillen@lanl.gov

Symbol: LANSCE-1:99-148

Date: August 10, 1999

SUBJECT: Superconducting Cavity Design for SNS

This memo reports a method for optimizing elliptical cavity shapes for potential use in a superconducting part of the SNS linac. The work was done at the request of Tom Wangler, who has been laying out a two-cavity-type superconducting linac.

Requirements

It is not the intention of the memo to justify all the parameter choices. However, I will, where appropriate, mention what kind of tradeoffs are involved.

In the present superconducting concept for SNS, the linac uses room-temperature structures up to a beam energy of 194 MeV. This energy corresponds to the end of a coupled-cavity linac rf module with an exit beam energy near ~200 MeV, below which elliptical niobium cavities are not as attractive because they are so short compared to their diameter. From previous design studies, we have already decided on two superconducting structure types. The first section uses a cavity with geometrical $\beta = 0.61$ to span the particle velocity range from $\beta = 0.560$ to 0.688 (194 MeV to 355 MeV). The other section uses a cavity with geometrical $\beta = 0.76$ for the range from $\beta = 0.688$ to 0.875 (355 MeV to 1 GeV).

Each cavity structure consists of eight cells operating in the π mode. One would like a large number of cells per cavity to reduce the number of rf drives and the number of control systems. However, for a given cell-to-cell coupling, increasing the number of cells per cavity degrades the field stability. If we can achieve ~2% cell-to-cell coupling in an 8-cell cavity, the field errors will be tolerable. An 8-cell cavity has six identical internal cells plus the two end cells. The inside wall of an end cell is the same as that of an internal cell. The outside walls will differ in shape for proper tuning. In addition, the bore tube on the end of the cavity is larger than the internal bore radius to help achieve sufficient coupling to the rf power supply. Previous work by Frank

may limit the performance of a superconducting cavity. In regions of high magnetic field, the surface may become normal conducting causing a quench, and in regions of high electric field, electron emission may occur. A discussion of the details of these effects is beyond the scope of this memo. For guidance in the design process, we apply the experience to date in achieving high fields. Henri Safa suggested a procedure that we have adopted for deciding whether a cavity will be limited by maximum E or B fields. First, define the maximum magnetic and electric fields (B_{MA} and E_{MA}) that have been achieved experimentally. (Ideally, these fields would correspond to the same cavity materials and fabrication techniques planned for the project of interest. Thus, the definitions are based upon subjective judgement to some extent.) Then, for a particular cavity design, compute the ratio B_{Max}/E_{Max} where B_{Max} is the peak magnetic field and E_{Max} is the peak electric field in the cavity at a given excitation level. If $B_{Max}/E_{Max} > B_{MA}/E_{MA}$, then the cavity is more likely to be limited by quenching and if $B_{Max}/E_{Max} < B_{MA}/E_{MA}$ the cavity is more likely to be limited by field emission. After discussions with Safa, Tom Wangler has chosen the following ratio for the present design effort:

$$\frac{B_{MA}}{E_{MA}} = \frac{120 \text{ mT}}{70 \text{ MV/m}} \approx 1.71 \frac{\text{mT}}{(\text{MV/m})}.$$

There are some mechanical constraints. For rigidity, we would like a wall angle in the range 6 to 9 degrees. Dale Schrage suggests that no radius of curvature in the cavity be smaller than about twice the material thickness for ease of forming the cavity. Niobium thickness values of 3 mm and 5 mm are being considered. However, some manufacturing techniques (e.g., spinning) would likely not have this requirement on the radii of curvature.

Cavity Design Features

We use the program ELLFISH in the Poisson Superfish code distribution to design the cavity shape and compute surface fields and rf power losses. Figure 1 shows the basic outline for half of an internal cell in a multicell elliptical cavity. The term “elliptical cavity” has become the common jargon used to refer to these cavities. As shown in the figure, a cross section of the right half of a cavity, the actual shape consists of a circular arc of radius R_c at the outer diameter, a sloping straight section at angle α_w from the vertical, and a segment of an ellipse of height $2b$ and width $2a$ near the bore. The lower left corner is the center of the cell. The left edge is the cavity midplane and the bottom edge is the beam axis. With appropriate boundary conditions, the half cavity is sufficient to model the interior cavities of a superconducting multicell cavity. The boundary conditions are Neumann at the left edge and Dirichlet at the right edge.

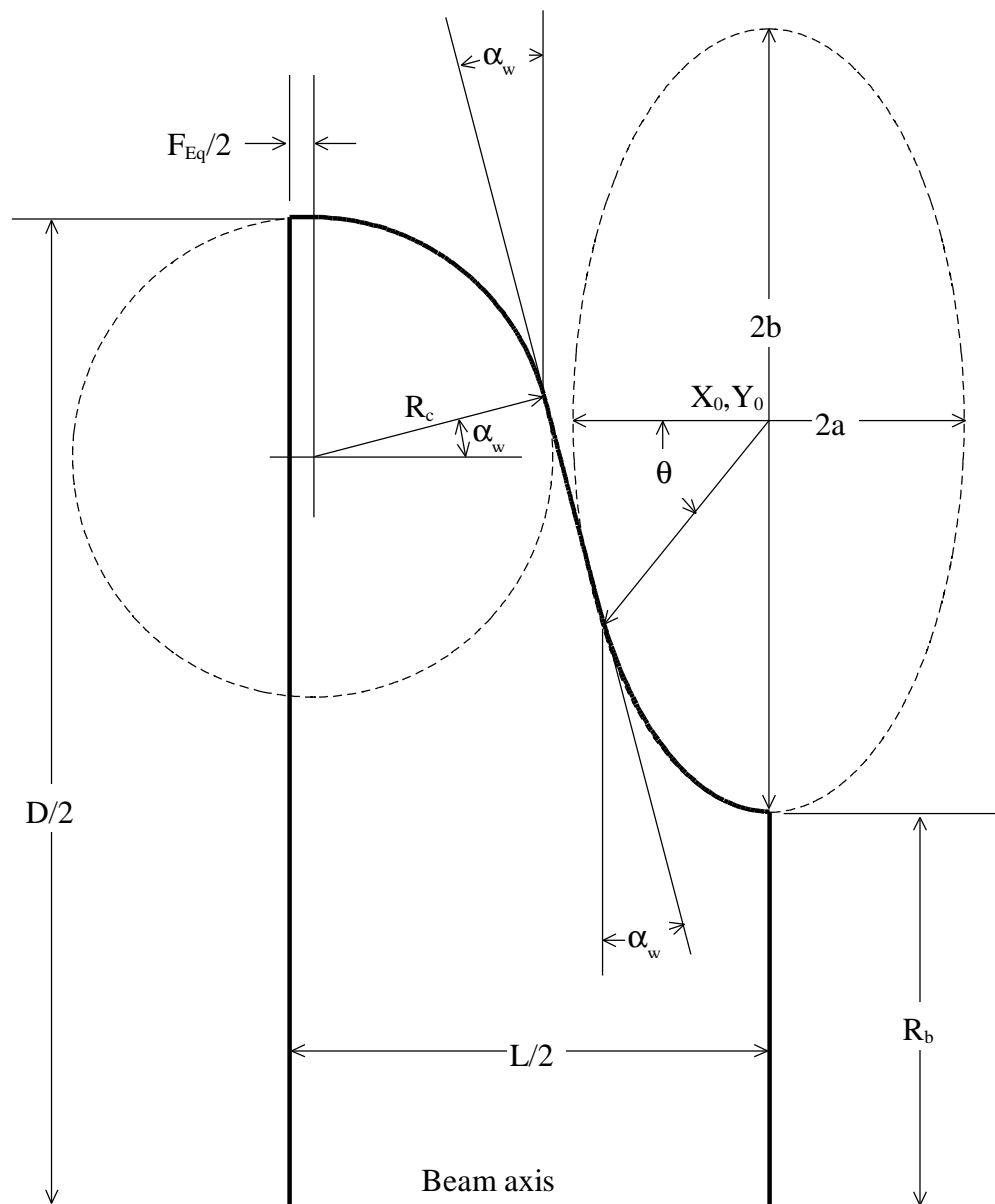


Figure 1. The right half of an elliptical cavity. The left edge is a symmetry plane with a

side. The bore tube of radius $R_{b,R}$ extends a distance δT_R beyond the nominal right edge of the cavity. If necessary, the geometry can include a second bore tube extension of length δT_2 and radius $R_{b,2}$. The cavity length is $L = \beta\lambda/2$, so the full length of the problem geometry is $L + \delta T_R + \delta T_2$. The code uses a Dirichlet boundary condition on the left and right edges of the problem geometry. On the right side, the bore tube is long enough so the fields fall to negligible values at the edge of the geometry. Neither Dirichlet nor Neumann boundaries would be appropriate at this edge.

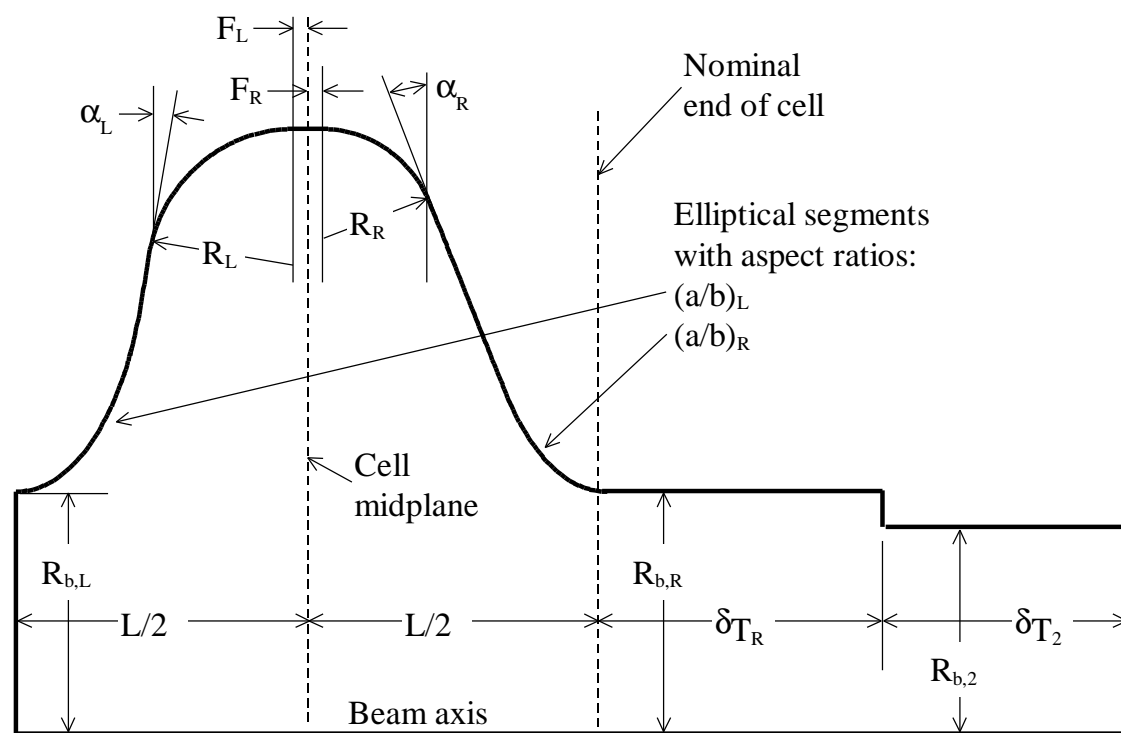


Figure 2. Full-cell elliptical cavity. The shape of the cavity wall on left and right can be different. The ELLFISH program can tune full cavities by adjusting the right-side radius or the right-side wall angle.

The only common parameters on left and right sides are the cavity diameter D and the half length $L/2$. As shown in Figure 2, all other parameters, including the ellipse aspect ratios, can have different values on the left and right sides. Even if $(a/b)_L = (a/b)_R$, the actual size of the two ellipse segments may be different depending on choices for the other geometrical parameters. The wall angle is α_L on the left and α_R on the right; the outer corner radius is R_L on the left and R_R on the

Program ELLFISH can tune the full-cell cavity by adjusting either the outer diameter D , the right-side corner radius R_R , or the right-side wall angle α_R . The usual procedure is to allow ELLFISH to tune the interior half cell by adjusting the cavity diameter for chosen settings of the other geometrical parameters. For the end cell, the designer fixes the geometry of the left side at the values found for interior cells and tunes the cell by adjusting the shape of the right-side cavity wall. The recommended method is to tune the full cavity by varying the right-side outer corner radius R_R .

Optimization Studies

For each design particle velocity ($\beta = 0.61$ and $\beta = 0.76$) we tuned a series of cavities with different choices for some of the geometrical parameters. The particle velocity fixes the length since $L = \beta\lambda/2$. At 805 MHz, the $\beta = 0.61$ cavity has a length of 11.3586 cm and the $\beta = 0.76$ cavity has a length of 14.1517 cm. The cell-to-cell coupling depends mainly on the cavity bore radius, but it also depends on the shape of elliptical segment between cavities. We investigated a few different bore radii and found adequate coupling with an internal bore radius $R_{b,L} = 5.0$ cm.

Optimizing the cavity to balance the peak surface fields involved varying the ellipse aspect ratio for several choices of the cavity corner radius R_c and the wall angle α_w . Figure 3 shows plots of the peak field ratio B_{Max}/E_{Max} versus the ellipse aspect ratio for three choices of R_c . The low- β cavity has $\alpha_w = 7$ degrees and the high- β cavity has $\alpha_w = 9$ degrees. The circled points are candidate cavities having the desired ratio $B_{Max}/E_{Max} \approx 1.71$ mT/(MV/m). At $\beta = 0.61$ nearly all of the points lie above this value. Cavities with aspect ratios smaller than ~ 0.35 become difficult to fabricate so we look to larger values of a/b . There is little room to increase R_c much beyond 3.2 cm, so we really have only one choice ($a/b = 1.5$) for the low- β cavity.

For the high- β cavity, Figure 3 shows three candidates with $B_{Max}/E_{Max} \approx 1.71$ mT/(MV/m). Obviously, it is possible to generate more cavities with this field ratio for any radius R_c between 4.5 and 5 cm. In order to choose among these cavities, we list in Table 1 the actual values of the peak fields and the cell-to-cell coupling for the three candidate cavities from Figure 3. The table shows that cavities 1 and 2 have substantially higher coupling than cavity 3 has. In terms of cavity fields, which have been normalized to $E_0T = 8.5$ MV/m, cavity 2 has a slight advantage over cavity 1 and a little larger advantage over cavity 3. Since there is little room to increase R_c much beyond 5.0 cm, we choose cavity 2 ($a/b = 0.9$) for the high- β cavity.

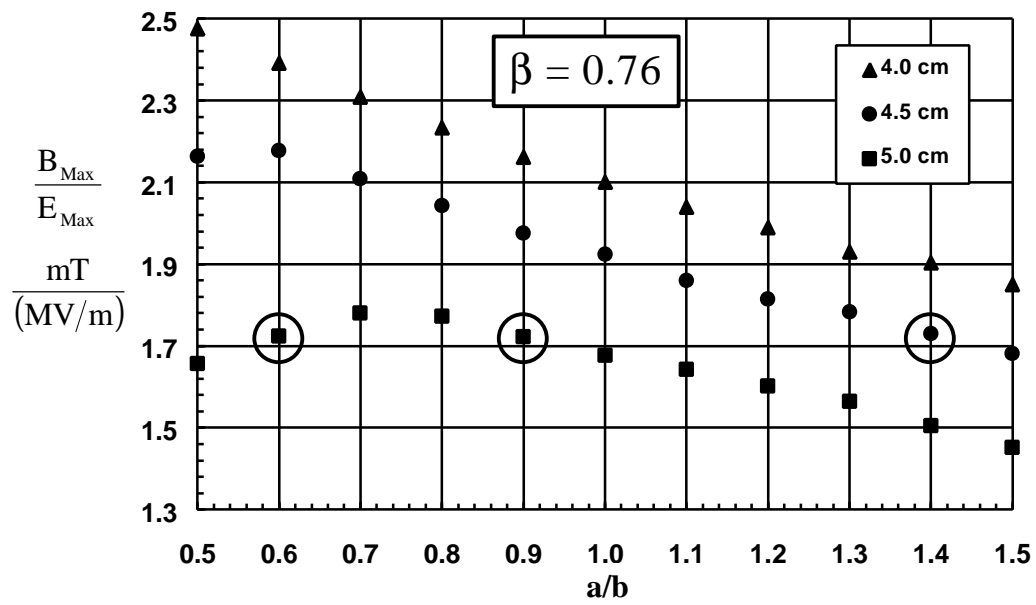
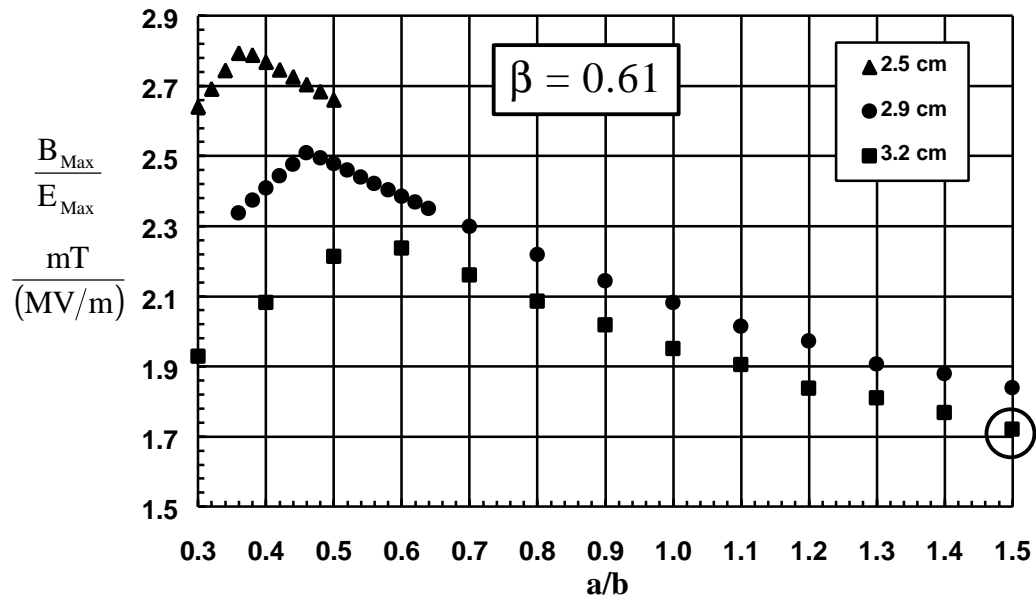


Figure 3. Ratio of maximum magnetic and electric fields versus ellipse aspect ratio for several cavities designed for each particle velocity. The indicated lengths are the

Table 1. Candidate cavities for $b = 0.76$.

| Parameter | Cavity 1 | Cavity 2 | Cavity 3 |
|-------------------|----------|----------|----------|
| a/b | 0.6 | 0.9 | 1.4 |
| R_c (cm) | 5.0 | 5.0 | 4.5 |
| H_{Max} (kA/m) | 32.16 | 31.95 | 33.26 |
| B_{Max} (mT) | 40.41 | 40.15 | 41.80 |
| E_{Max} (MV/m) | 23.45 | 23.32 | 24.17 |
| B_{Max}/E_{Max} | 1.72 | 1.72 | 1.73 |
| Coupling (%) | 2.18 | 2.09 | 1.54 |

Design Parameters for SNS

Having chosen the basic shape of the internal cells, we proceeded to design the end cavity for the 8-cell structure. As illustrated by Figure 2, which shows the end cavity on the right-hand side of the structure, we make the end cavity's inner-wall shape identical to the shape of the internal cells. If we did the same for the outer wall, the frequency of the end cavity would be a few MHz lower than the internal cells because of the electric fields penetrating into the bore tube. We raise the frequency of the end cell by reducing the corner radius R . Table 2 lists cavity parameters for both design velocities. Refer to Figures 1 and 2 for definitions of symbols listed for the geometric parameters.

After tuning the internal cell and the end cell to 805 MHz, we construct the geometry for half of the 8-cell cavity and run SUPERFISH to compute the frequencies and axial field distributions for all eight modes in the TM_{010} pass band. Figure 4 is a plot of field contours computed by SUPERFISH for the 805-MHz mode of each cavity. Figure 5 shows the eight axial field distributions in the $\beta = 0.61$ cavity. The patterns are nearly identical for the $\beta = 0.76$ cavity. The field plots correspond to the right half of the cavity. Each mode in the TM_{010} passband is labeled by its phase coordinate on the dispersion curve (see Figure 6), which was fitted by the program DISPER. Frequencies of all the modes appear in Table 3. Although it is common practice to refer to the highest frequency mode as the π mode," this term properly applies only to an infinitely long structure. The curves plotted in Figure 6 correspond to a finite number of cavities (eight) terminated by full cells. The values of the nearest neighbor coupling k and second neigh

Table 2. Cavity Parameters.

| Parameter | Symbol | $\beta = 0.61$ | $\beta = 0.76$ |
|---|---------------------------|----------------|----------------|
| Nominal cell length (cm) | L | 11.3586 | 14.1517 |
| Cavity diameter (cm) | D | 33.1629 | 33.0032 |
| Internal cell (left side) bore radius (cm) | $R_{b,L}$ | 5.0 | 5.0 |
| External (right side) bore radius (cm) | $R_{b,R}$ | 5.5 | 5.5 |
| Internal cell (left side) corner radius (cm) | R_L | 3.2 | 5.0 |
| External (right side) corner radius (cm) | R_R | 3.1382 | 4.5794 |
| Wall angle (degrees) | α_L | 7.0 | 9.0 |
| Equator flat length (cm) | F_{Eq} | 0.0 | 0.0 |
| Ellipse aspect ratio | a/b | 1.50 | 0.90 |
| Ellipse center to mid cell on left side (cm) | $X_{0,L}$ | 5.6793 | 7.0758 |
| Ellipse center to axis on left side (cm) | $Y_{0,L}$ | 6.0318 | 6.3022 |
| Horizontal semi-axis on left side (cm) | a_L | 1.5477 | 1.1720 |
| Vertical semi-axis on left side (cm) | a_R | 1.0318 | 1.3022 |
| Ellipse center to mid cell on right side (cm) | $X_{0,R}$ | 5.6793 | 7.0758 |
| Ellipse center to axis on right side (cm) | $Y_{0,R}$ | 6.6158 | 7.3825 |
| Horizontal semi-axis on right side (cm) | b_L | 1.6736 | 1.6943 |
| Vertical semi-axis on right side (cm) | b_R | 1.1158 | 1.8825 |
| External beam tube length (cm) | δT_R | 12.5 | 12.5 |
| Second beam tube length (cm) | δT_2 | 10.0 | 10.0 |
| Second beam tube radius (cm) | $R_{b,2}$ | 4.2 | 4.2 |
| Frequency (MHz) | $f_{8\pi/9}$ | 805.000 | 805.000 |
| Nearest neighbor coupling (%) | k | 2.037 | 2.194 |
| Second neighbor coupling (%) | k_2 | 0.205 | 0.199 |
| Frequency difference to nearest mode (kHz) | $f_{8\pi/9} - f_{7\pi/9}$ | 575 | 642 |

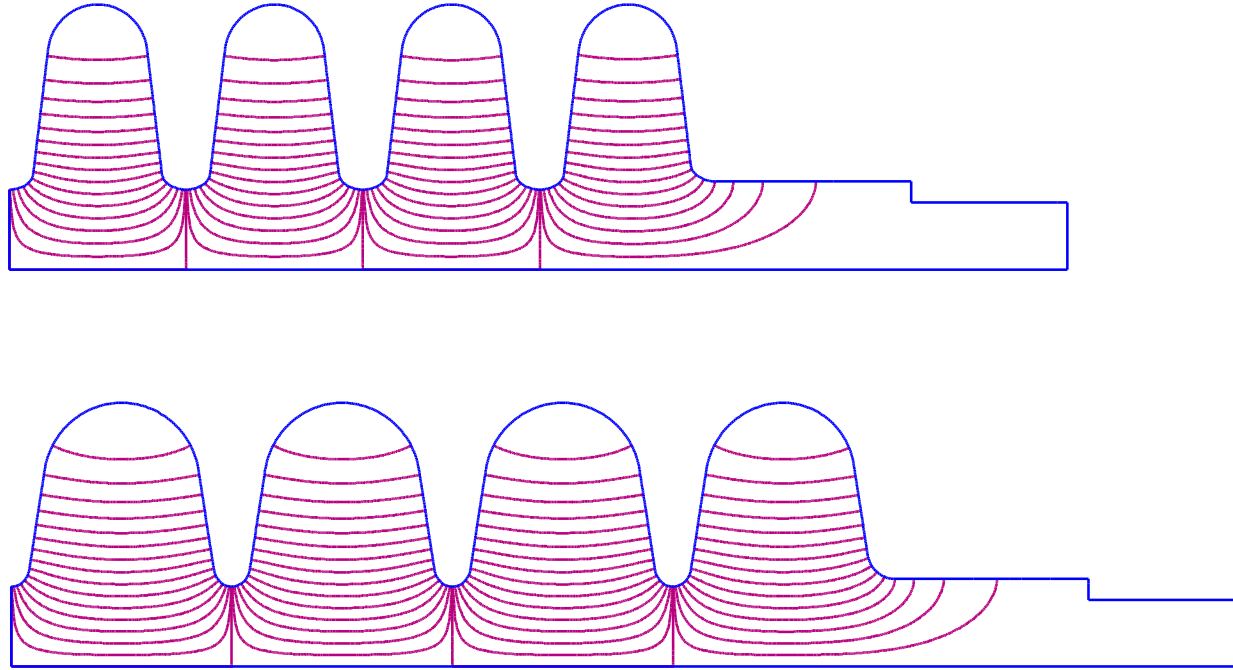
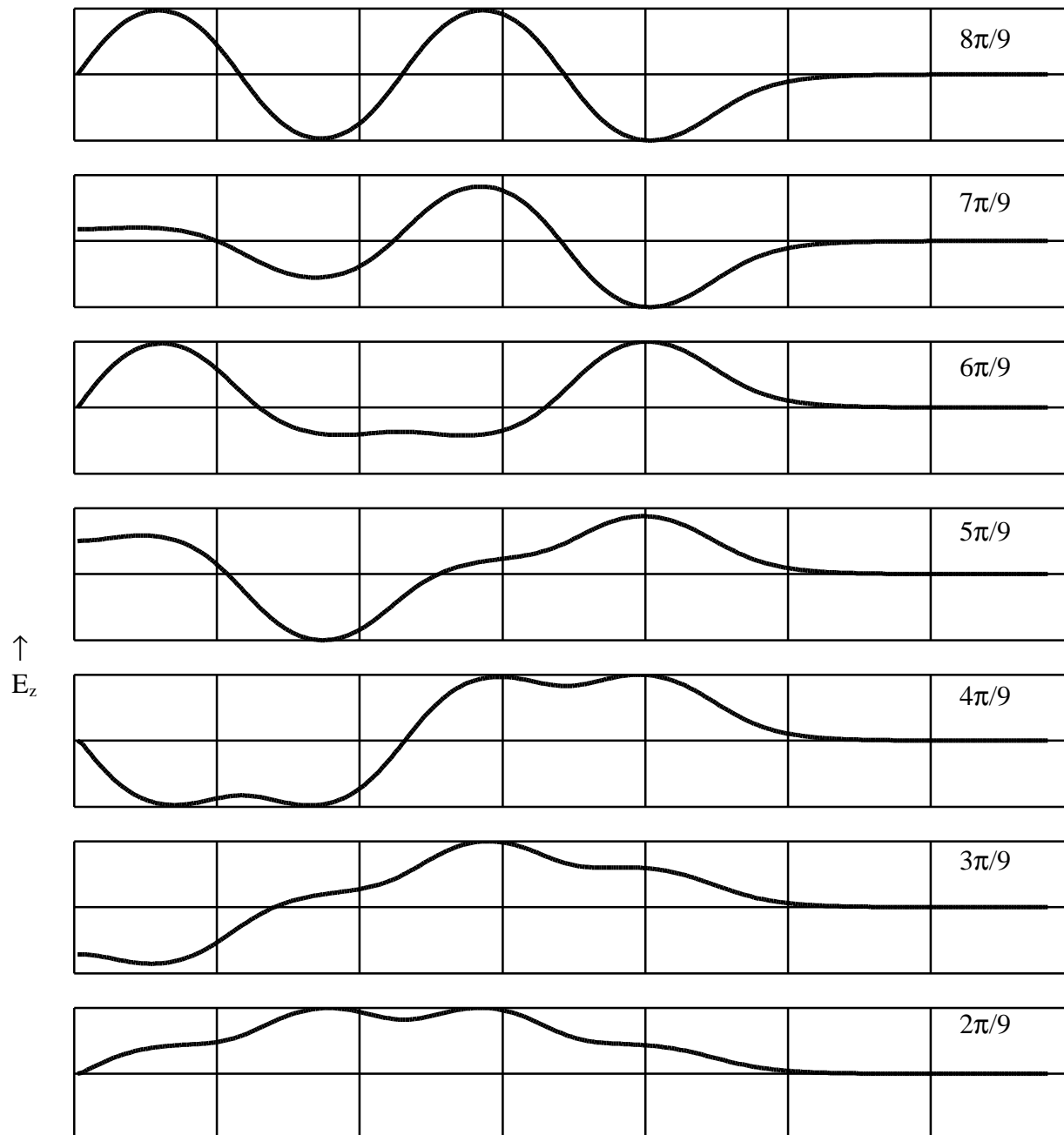
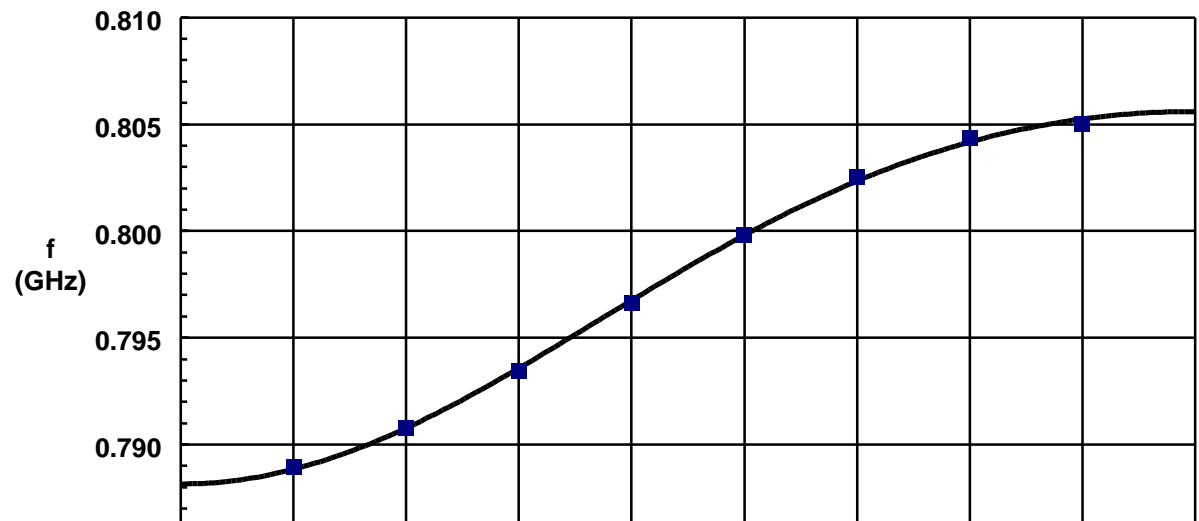
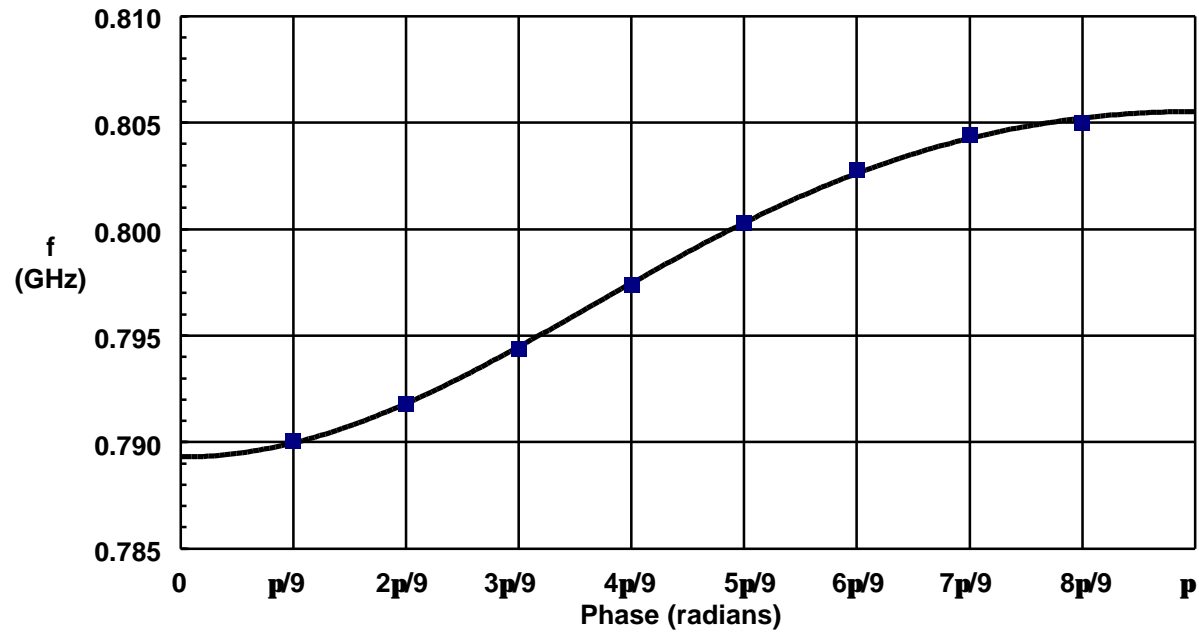


Figure 4. SUPERFISH generated cavity shapes for $b = 0.61$ (top) and $b = 0.76$ (bottom) for half of an 8-cell cavity. The contour lines correspond to constant values of the magnetic field H_f . The electric field is parallel to these contours.

Table 3. Mode frequencies in MHz for the TM_{010} pass band.

| Phase | $\beta = 0.61$ | $\beta = 0.76$ |
|----------|----------------|----------------|
| $\pi/9$ | 790.070 | 788.966 |
| $2\pi/9$ | 791.798 | 790.756 |
| $3\pi/9$ | 794.361 | 793.442 |
| $4\pi/9$ | 797.252 | 796.622 |





Transit-Time Factors

The energy gain of a charged particle through a cavity is

$$\delta W = qE_0 A b s (T + iS) \cos \phi_s L,$$

where q is the charge, L is the cell length, and ϕ_s is the synchronous phase. The quantity E_0 is the average axial electric field given by

$$E_0 = \frac{1}{L} \int_{Z_s}^{Z_e} |E_z| dz,$$

where Z_s and Z_e are starting and ending longitudinal coordinates that span the nonzero axial fields of the cavity. Variables T and S are the real and imaginary parts of the transit-time factor, which are defined as follows:

$$T = \frac{1}{E_0 L} \int_{Z_s}^{Z_e} E_z(z) \cos[k(z - Z_c)] dz,$$

and

$$S = \frac{1}{E_0 L} \int_{Z_s}^{Z_e} E_z(z) \sin[k(z - Z_c)] dz,$$

where $k = 2\pi/\beta\lambda$ is the wave number, and $\beta\lambda$ is the distance traveled in one rf period by a particle of velocity βc . The resonant mode has frequency $f = c/\lambda$, where λ is the free-space wavelength. For beam dynamics simulations in the superconducting part of a linac, one needs the transit-time factors as a function of particle velocity. The postprocessor program SFO in the Poisson Superfish code distribution computes T and S as well as their derivatives with respect to the wave number k :

$$T' = \frac{1}{E_0 L^2} \int_{Z_s}^{Z_e} (z - Z_c) E_z(z) \sin[k(z - Z_c)] dz,$$

$$S' = \frac{1}{E_0 L^2} \int_{Z_s}^{Z_e} (z - Z_c) E_z(z) \cos[k(z - Z_c)] dz,$$

Table 4. Transit-time factors for $b = 0.61$ cavity.

| β | S | S' | S'' |
|---------|----------|-----------|-----------|
| 0.50 | 0.073793 | -0.404288 | -0.476691 |
| 0.51 | 0.139670 | -0.470249 | -0.395158 |
| 0.52 | 0.211400 | -0.519741 | -0.284747 |
| 0.53 | 0.286026 | -0.550394 | -0.152143 |
| 0.54 | 0.360670 | -0.561082 | -0.004699 |
| 0.55 | 0.432692 | -0.551799 | 0.150138 |
| 0.56 | 0.499797 | -0.523489 | 0.305292 |
| 0.57 | 0.560093 | -0.477843 | 0.454391 |
| 0.58 | 0.612124 | -0.417100 | 0.591993 |
| 0.59 | 0.654866 | -0.343852 | 0.713707 |
| 0.60 | 0.687703 | -0.260875 | 0.816229 |
| 0.61 | 0.710389 | -0.170984 | 0.897315 |
| 0.62 | 0.723000 | -0.076911 | 0.955703 |
| 0.63 | 0.725880 | 0.018778 | 0.991012 |
| 0.64 | 0.719591 | 0.113754 | 1.003615 |
| 0.65 | 0.704856 | 0.205965 | 0.994505 |
| 0.66 | 0.682518 | 0.293655 | 0.965169 |
| 0.67 | 0.653494 | 0.375379 | 0.917461 |
| 0.68 | 0.618739 | 0.449989 | 0.853489 |
| 0.69 | 0.579216 | 0.516626 | 0.775517 |
| 0.70 | 0.535869 | 0.574696 | 0.685876 |
| 0.71 | 0.489606 | 0.623843 | 0.586893 |
| 0.72 | 0.441281 | 0.663925 | 0.480833 |
| 0.73 | 0.391685 | 0.694984 | 0.369857 |
| 0.74 | 0.341539 | 0.717215 | 0.255979 |
| 0.75 | 0.291490 | 0.730944 | 0.141053 |
| 0.76 | 0.242107 | 0.736594 | 0.026751 |
| 0.77 | 0.193887 | 0.734673 | -0.085446 |
| 0.78 | 0.147252 | 0.725743 | -0.194242 |
| 0.79 | 0.102554 | 0.710405 | -0.298532 |
| 0.80 | 0.060082 | 0.689286 | -0.397389 |

Table 5. Transit-time factors for $b = 0.76$ cavity.

| β | S | S' | S'' |
|---------|-----------|-----------|-----------|
| 0.60 | -0.025149 | -0.271450 | -0.558731 |
| 0.61 | 0.014994 | -0.343526 | -0.541675 |
| 0.62 | 0.062590 | -0.409505 | -0.499097 |
| 0.63 | 0.116234 | -0.466734 | -0.433100 |
| 0.64 | 0.174358 | -0.513122 | -0.346703 |
| 0.65 | 0.235327 | -0.547172 | -0.243568 |
| 0.66 | 0.297510 | -0.567968 | -0.127735 |
| 0.67 | 0.359351 | -0.575140 | -0.003392 |
| 0.68 | 0.419419 | -0.568804 | 0.125325 |
| 0.69 | 0.476437 | -0.549496 | 0.254490 |
| 0.70 | 0.529314 | -0.518096 | 0.380508 |
| 0.71 | 0.577151 | -0.475752 | 0.500199 |
| 0.72 | 0.619246 | -0.423803 | 0.610855 |
| 0.73 | 0.655089 | -0.363718 | 0.710259 |
| 0.74 | 0.684349 | -0.297030 | 0.796692 |
| 0.75 | 0.706864 | -0.225284 | 0.868914 |
| 0.76 | 0.722617 | -0.149997 | 0.926137 |
| 0.77 | 0.731723 | -0.072620 | 0.967983 |
| 0.78 | 0.734405 | 0.005491 | 0.994438 |
| 0.79 | 0.730979 | 0.083089 | 1.005809 |
| 0.80 | 0.721830 | 0.159056 | 1.002668 |
| 0.81 | 0.707398 | 0.232407 | 0.985806 |
| 0.82 | 0.688164 | 0.302294 | 0.956189 |
| 0.83 | 0.664633 | 0.368005 | 0.914911 |
| 0.84 | 0.637320 | 0.428959 | 0.863156 |
| 0.85 | 0.606744 | 0.484703 | 0.802166 |
| 0.86 | 0.573417 | 0.534901 | 0.733207 |
| 0.87 | 0.537835 | 0.579323 | 0.657544 |
| 0.88 | 0.500474 | 0.617841 | 0.576420 |
| 0.89 | 0.461784 | 0.650411 | 0.491037 |
| 0.90 | 0.422189 | 0.677069 | 0.402543 |

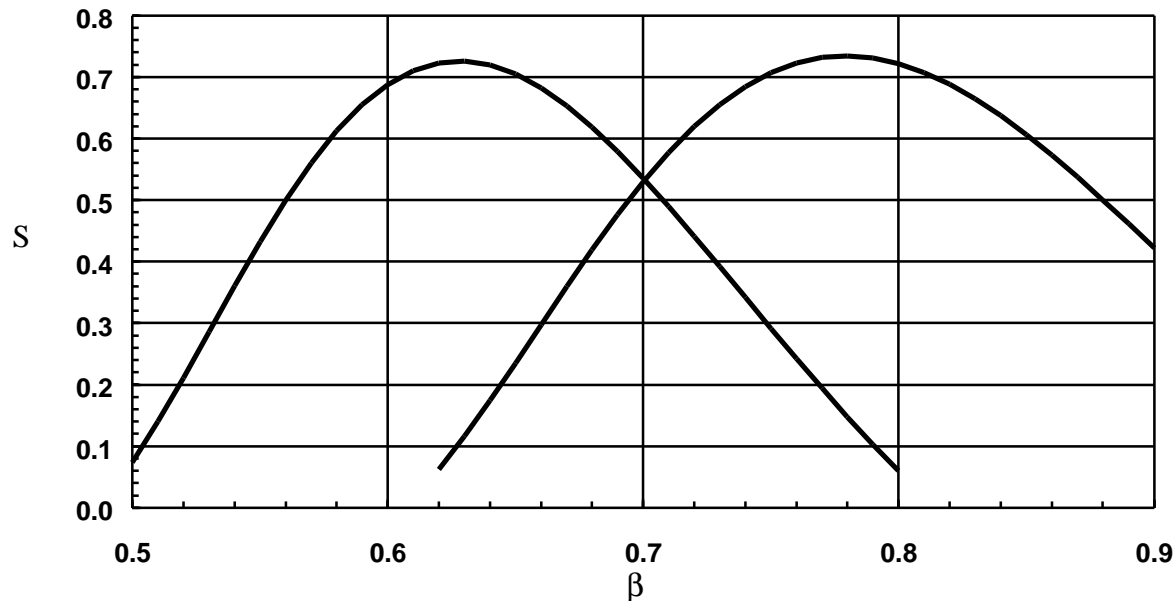


Figure 7. Whole-cavity transit-time factors for both 8-cell elliptical cavities. The curve on the left corresponds to the $b = 0.61$ cavity and the curve on the right corresponds to the $b = 0.76$ cavity.

Some beam dynamics codes such as PARMILA step the particles through each cell of the structure, applying impulses at the center of each cell. For input to PARMILA, SFO generates transit-time-factor data in a series of files, one file for each specified particle velocity. Another utility program reads this family of files and creates “SFDATA” tables to include in the PARMILA input file. Though these data are too numerous to list in this memo, they will be available by electronic transfer as described below.

Data Files

The SUPERFISH input and output files for the elliptical cavities are available in shared directories \\pc-billen\Projects\NSNS\SC\beta.61 and \\pc-billen\Projects\NSNS\SC\beta.76. (If you are not a member of the AOT-1 computer domain, log in to machine pc-billen.atdiv.lanl.gov by FTP as user Linac with password aot1ftn.)

Electronic Distribution:

A. J. Jason, LANSCE-1, ajason@lanl.gov
F. L. Krawczyk, LANSCE-1, fkrawczyk@lanl.gov
S. S. Kurennoy, LANSCE-1, kurennoy@lanl.gov
T. S. Bhatia, LANSCE-1, tsb@lanl.gov
R. D. Ryne, LANSCE-1, ryne@lanl.gov
J. Qiang, LANSCE-1, jiqiang@lanl.gov
S. Nath, LANSCE-1, snath@lanl.gov
J. D. Gilpatrick, LANSCE-1, gilpatrick@lanl.gov
R. Garnett, LANSCE-1, rgarnett@lanl.gov
D. L. Schrage, LANSCE-1, dls@lanl.gov
H. Takeda, LANSCE-1, htakeda@lanl.gov
T. P. Wangler, LANSCE-1, twangler@lanl.gov
M. T. Lynch, LANSCE-5, mtlynch@lanl.gov
P. J. Tallerico, LANSCE-5, tallerico@lanl.gov
N. K. Bultman, ESA-EA, nbultman@lanl.gov
P. Grand, TechSource, pgrand@ibm.net
R. B. Miller, SNS-PO, rbmiller@lanl.gov
J. E. Stovall, SNS-PO, jstovall@lanl.gov
B. K. Hartline, SNS-PO, hartline@lanl.gov
R. A. Hardekopf, SNS-PO, hardekopf@lanl.gov

Hard Copy Distribution:

S. O. Schriber, LANSCE-DO, H850
LANSCE-1 Reading File, H808
LANSCE-DO, H850
SNS Project Office, H824